Egyptian Journal of Geology
https://egjg.journals.ekb.eg

Durability Assessment of Ooidal Ironstones in Aswan Region, Egypt

Hesham A.H. Ismaiel[a], Karem M. Moubarak[a], Karam A .Abdelkader [b] and **Ali I. Ali[a]***

[a]*Department of Geology, Faculty of Science, South Valley University, 83511 Qena, Egypt*
[b]*Geo-Quarry Mining Co., Commercial Street, El Corniche, 81511 Aswan, Egypt*

Ooidal ironstone, a sedimentary rock present in Aswan region of Egypt, its slaking durability susceptibility poses questions to its long-term performance and suitability for construction and infrastructure applications. In this study, the slaking behavior of ooidal ironstones of Timsah Formation are examined using the standard slake-durability test. A detailed analysis on their physical, chemical, and mineralogical characteristics was conducted to identify key controlling factors. The experimental results indicate that ooidal ironstones possess medium-high to high slaking durability indices (I_{d_2}: 92.51–96.74%). Slaking durability was found to be strongly correlated with certain factors such as mineral composition, especially the occurrence of apatite and kaolinite and physical characteristics such as porosity, bulk density, and water absorption. Besides, it was also especially influenced by geochemical aspects such as Fe_2O_3, P_2O_5, and CaO contents. The study concluded that the studied ooidal ironstone can be showed potential for specialized uses such as aggregates for high-performance concrete in radiation-shielding structures. Additionally, non-destructive testing approaches, specifically ultrasonic P-wave velocity (UPV), exhibit a strong correlation with slake durability index ($R^2 > 0.76$), providing a practical tool for field assessments.

Keywords: Ooidal ironstone, slaking durability, mineralogy, geochemistry, index properties.

1. Introduction

Ooidal ironstone, which is an iron mineral-rich sedimentary rock, usually hematite (Fe_2O_3) and goethite (FeO(OH)), has more than 5% ooids and more than 15% iron content (Young, 1990; Petránek and Van **Houten, 1997**; Mücke and Farshad, 2005).

Despite the presence of a large reserve estimated at approximately nine million tons, the use of ooidal ironstones in the Aswan region for local steel production is hampered by the presence of fine silicate minerals and high phosphorus levels (Hussein and Sharkawi, 1990; Mücke, 2000; Baioumy et al., 2017). However, Aswan's ooidal ironstones are economically valuable and are utilized in a great number of various industries.

The geotechnical evaluation of ironstone is necessary in determining its suitability for construction purposes (Nwaiwu et.al., 2006). In this evaluation, various aspects are taken into consideration, such as porosity, density, durability, and strength. Furthermore, geotechnical evaluations of ironstone play a pivotal role in comprehending its geotechnical attributes in the context of mining operations (e.g., **Hanson et.al., 2005**; Hu et.al., 2017). This includes the evaluation of optimal blasting techniques, excavation sequences, and waste management strategies to ensure the practice of safe and sustainable mining (Bamber, 2008; Balamadeswaran and Mishra, 2020; Rahimi et.al., 2021).

Extensive geological investigations have been carried out on the ooidal ironstones of Aswan area including various disciplines such as mineralogy, sedimentology, petrography, stratigraphy, and geochemistry (e.g., Klitzsch, 1986; Bhattacharyya, 1989; El Aref et al., 1996; Mücke, 2000; Salama, 2014; Baioumy et al., 2017). Despite the large number of investigations in these fields, there is a severe shortage of such comprehensive investigations related to its geotechnical properties, particularly to slaking durability. This work attempts to fill this gap through examining the slaking durability of the Ooidal ironstones and its key controlling factors.

2. Materials and Methods

2.1 Materials

The study area is situated in the vicinity of Wadi Abou Aggag, located northeast of Aswan City, Egypt. It

*Corresponding author e-mail: Ali.ismail2@sci.svu.edu.eg
Received: 20/05/2025; Accepted: 10/07/2025
DOI: 10.21608/EGJG.2025.387394.1114

extends between latitudes 24° 3' 45" – 24° 16' 12" N and longitudes 32° 51' 11" – 33° 8' 52" E, which covering about 685 km^2 (Fig. 1). This region displays a wide range of lithological units covering different geological ages, namely, the Quaternary, Miocene, Cretaceous, and Pre-Cambrian (e.g. Klitzsch, 1986, Bhattacharyya, 1989, El Aref et al., 1996, Mücke, 2000).

Near Wadi Abou Aggag, Timsah Formation consists of reddish grey and yellowish grey laminated mudstone with massive ironstone intercalations of what is known as "Aswan clays". Overlying the mudstone sequence, two intercalated ooidal ironstone beds are separated, the lower is 2 meters thick, while the upper reaches a thickness of about 4 meters. Separating these two layers a shale layer, 30 cm thick, ranging in color from yellowish to reddish gray (Mekkawi et al., 2021; Youssef, 2018; Baioumy et al., 2017).

Eight oriented block samples were collected from four mining sites (S1, S2, S3 and S4) in the vicinity of Wadi Abou Aggag from different open pit mines (Fig. 2).

The collected samples represent only Ooidal ironstones litho-type of Timsah Formation. Two-block samples were collected from the lower and upper ooidal ironstones beds in each site, the dimensions of the collected block samples are not less than 25 cm. Samples were identified systematically with a code such as S1A, S2B, etc. Here, 'S' represents the sampling locality, with the succeeding number representing the mining locality (e.g., '1' for the first mining locality). The last letter represents the stratigraphic position: 'A' representing the lower ooidal ironstone bed, and 'B' representing the upper ooidal ironstone bed.

Fig. 2. A photograph shows the upper part of Timsah Formation at Wadi Abu Aggag (24°57′ 37.00″N, 46°11′ 33.00″E).

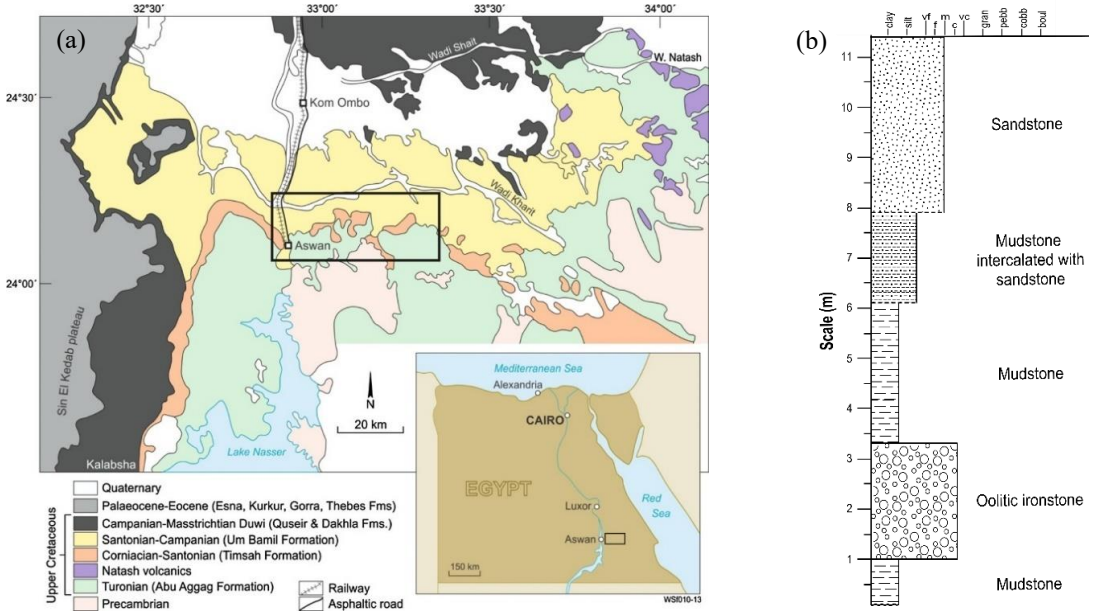

Fig. 1. (a) A simplified geological and location map of Aswan region, after Klitzsch et al. 1987, modified by Salama, 2014; (b) A simplified stratigraphic section of the exposed Timsah Formation in the in the vicinity of Wadi Abou Aggag.

2.2 Methods

The collected samples were subjected to analysis for their bulk mineralogical composition using the X-ray diffraction (XRD) technique by GBC Emma X-ray diffractometer (Cu Kα, 40 kV, 30 mA). The X-ray spectrometer (XRF) is used to analyze the studied samples for their major oxides (SiO_2, TiO_2, Al_2O_3, Fe_2O_3, MnO, MgO, CaO, K_2O, Na_2O, and P_2O_5). XRD and XRF analyses were performed at the Central

Laboratory of Faculty of Science, South Valley University, Qena, Egypt.

The saturation and caliper technique as outlined in ISRM (Brown, 1981) was used to determine the bulk density and porosity values. The ultrasonic pulse velocity (UPV) measurements were conducted using a V-Meter (Mark III) ultrasonic tester equipped with a 54 kHz transducer and following ISRM standards (Aydin, 2014). For these tests, three cylindrical specimens were prepared from each block sample, each with a diameter of 45 mm and a length of 100 mm. Furthermore, direct Schmidt hammer testing was performed on each block sample following ISRM protocols (Aydin, 2009).

The slaking durability tests were performed according to ISRM (Brown, 1981), using A130 Matest™ slaking durability device. The relationship between slaking durability index and weathering grade was determined following the classification scheme developed by Gamble (1971) and recommended by ISRM (Ulusay and Hudson, 2007). The slaking durability test was recommended to continue till only two-cycles as suggested by ISRM to describe the short-term effect of wetting and drying, but to evaluate the long-term slaking behavior of the studied iron ore. The test was performed till the fourth cycle (I_{d4}) as suggested by different workers (e.g., Gökceoglu et al., 2000; Selen et al., 2020; Zorlu and Yağiz, 2018).

The slaking durability index value does not consider the nature of fragmentation of a particular rock type (Erguler and Ulusay, 2009). To minimize this fundamental limitation, the material retained after each slaking durability test was photographed, and the results were compared with the ASTM (1996) visual classification system. These experiments were carried out at the Engineering Geology Laboratory, Faculty of Science, South Valley University, Qena, Egypt.

3. Results and Discussions

3.1 Mineralogy

The results of XRD analysis of the bulk mineralogy showed that the studied samples are composed mainly of hematite and quartz minerals, with minor or trace minerals including kaolinite and apatite in S1A, kaolinite and goethite in S2A, apatite in both S3A and S3B, and rutile in S4A (Table 1). Diffractograms of some representative samples were illustrated in Figure 3.

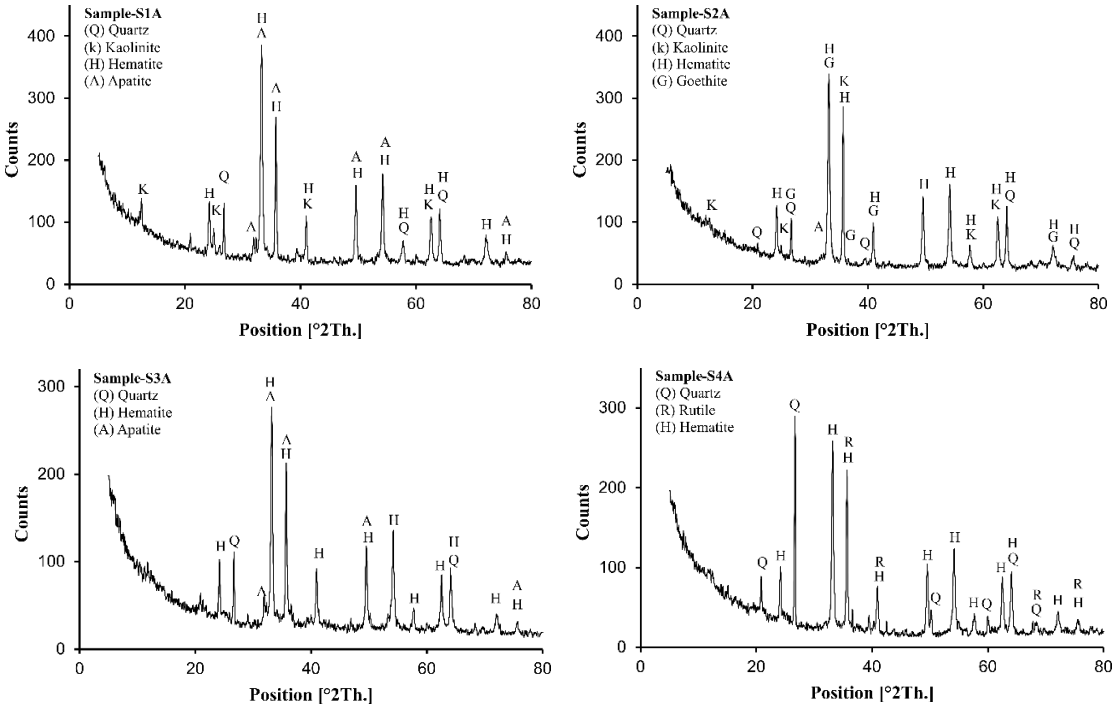

Fig. 3. X-ray diffractograms of some representative studied samples show the bulk mineralogy.

Table 1. XRD analysis results of the bulk minerals.

Samples	Minerals					
	Hem.	Qz.	Ge.	Ka.	Ap.	Ru.
S1A	✓	✓		✓	✓	
S1B	✓	✓		✓		
S2A	✓	✓	✓			
S2B	✓	✓		✓		
S3A	✓	✓	✓		✓	
S3B	✓	✓			✓	
S4A	✓	✓				✓
S4B	✓	✓		✓	✓	✓

3.2 Geochemistry

The chemical analysis of the analyzed samples indicated that the most abundant oxide is Fe_2O_3, varying from 66.48 to 76.51 % and an average of 70.28 %. The second most abundant oxide is SiO_2, varying between 13.14 and 28.02 % and an average of 18.75 %, followed by Al_2O_3 ranged from 3.23 to 6.54 % with an average of 4.65 %. CaO contents ranged from 0.67 to 5.61 % (average of 1.24 %) and P_2O_5 ranged from 0.59 to 2.65 % and an average of 0.64 % (Table 2).

Generally, the chemical composition of the studied samples is unsuitable for direct steel production despite the high Fe_2O_3 content. Its potential utilization by the Egyptian steel industry for domestic steel production is quite problematic due to the dissemination of fine silicate minerals and elevated phosphorus content, exceeding the desired 0.1% (Baioumy et al., 2017). For steel production, the phosphorus content should ideally be below 0.1% (Singh et al., 2024). Despite these complexities, Aswan's ooidal ironstones possess great economic importance and find application in a wide range of industries.

Table 2. Major oxides assay (wt. %) and loss on ignition (L.O.I. %) of the studied samples.

Oxides (wt.%)	Samples								Max.	Min.	Ave.
	S1A	S1B	S2A	S2B	S3A	S3B	S4A	S4B			
Na_2O	0.00	0.00	0.00	0.00	0.00	0.00	0.00	0.00	0.00	0.00	0.00
K_2O	0.10	0.02	0.09	0.05	0.05	0.03	0.10	0.10	0.10	0.02	0.07
Al_2O_3	3.26	6.54	3.41	4.21	3.23	4.26	5.16	4.65	6.54	3.23	4.34
SiO_2	13.14	28.02	14.07	14.25	15.82	16.21	20.76	18.75	28.02	13.14	17.63
P_2O_5	2.31	0.72	0.73	0.59	2.11	2.65	0.73	0.64	2.65	0.59	1.31
SO_3	0.26	0.22	0.23	0.24	0.28	0.19	0.32	0.23	0.32	0.19	0.25
Cl	0.08	0.08	0.10	0.09	0.07	0.07	0.06	0.05	0.10	0.05	0.08
MgO	0.24	0.42	0.38	0.58	0.54	0.60	0.46	0.57	0.60	0.24	0.47
CaO	5.61	0.69	1.33	0.82	4.40	4.23	0.67	1.24	5.61	0.67	2.37
TiO_2	0.33	0.28	0.35	0.32	0.28	0.37	0.45	0.55	0.55	0.28	0.37
MnO_2	0.09	0.22	0.05	0.25	2.35	0.14	0.32	0.35	2.35	0.05	0.47
Fe_2O_3	72.13	59.20	76.51	74.95	66.48	67.87	66.95	70.28	76.51	59.20	69.30
L.O.I.	2.30	3.50	2.60	3.50	4.30	3.30	4.00	2.45	4.30	2.30	3.24
SUM.	99.85	99.91	99.85	99.85	99.91	99.92	99.98	99.86	---	---	----

3.3 Porosity, Density, and Absorption

The results of the tests for porosity and density showed that the studied ooidal ironstones have a wide range of bulk density (2.33 to 2.88 g/cm3), solid density (3.58 to 3.79 g/cm^3), and porosity (18.49 to 26.60 %). The average bulk density, solid density, and porosity are 2.86 g/cm^3, 3.73 g/cm^3, and 28.32 %, respectively.

The total water absorption of the samples studied is relatively high, it ranges from 6.51 to 9.89 %, while its average value is 8.50 %. The high total water absorption of the studied ooidal ironstones is due to its high porosity. It means that the ooidal ironstones are susceptible to water damage. The porosity, density, and absorption properties of the studied ooidal ironstones align with the results for similar ooidal ironstone deposits (e.g. Daoud et al., 2020).

The low bulk density and high porosity of the ooidal ironstones can be attributed to and consistent with its ooidal texture. The wide range of bulk density and porosity values suggesting that the studied ooidal ironstones samples are mainly heterogenous and may have undergone different diagenetic processes.

The high determination coefficient ($R^2 = 0.76$) for the linear regression between porosity and bulk density (Fig. 4) indicates that there is a strong correlation between these two properties. This suggests that the porosity of the ooidal ironstone is the primary factor that controls its bulk density. The strong correlation between porosity and bulk density can be used to develop predictive models for estimating the porosity of the studied ironstone samples from their bulk density. However, linear regression of bulk density against solid density exhibits low determination

coefficient (R2=0.19) which shows that the solid density is not having a considerable influence on the bulk density.

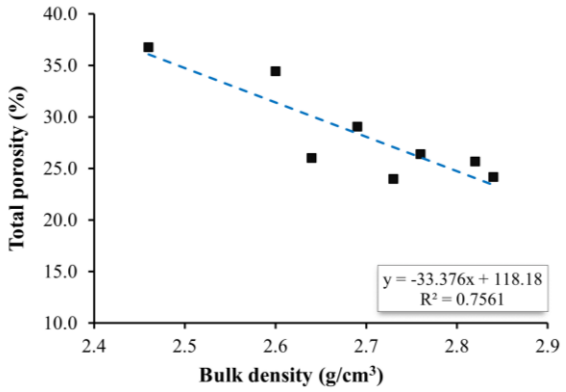

Fig. 4. Scatter plots and regression analysis of total porosity and bulk density.

3.4 Ultrasonic P-Wave Velocity

The ultrasonic P-wave velocity (UPV) test results show that most of the studied samples have high UPV values, varying from 1911 to 3275 m/s, and an average of 2590 m/s.

The low determination coefficient ($R^2 = 0.21$) in the linear regression between UPV and bulk density values suggests that there are other factors that influence the UPV of the studied ooidal ironstone in addition to bulk density. These factors include the porosity of the material, the presence of cracks or other defects, and the presence of impurities. This wide range can be due to several factors, such as rock strength and integrity, effective stress, mineral composition, granular structure, cementation, porosity, lithology, saturation, micro-cracks **(Horsfall et al., 2013)**.

3.5 Schmidt's Rebound Number (SRN)

The values of SRN or Schmidt's hardness of the studied samples vary between 21.45 and 33.67, while their average values are 27.54. The SRN and density values are used for predicting the uniaxial compressive strength (UCS) employing the proposed chart by Deere and Miller (1966). The estimated values of UCS vary between 32.35 MPa and 62.11MPa, while their average value is 44.69 MPa (Table 3).

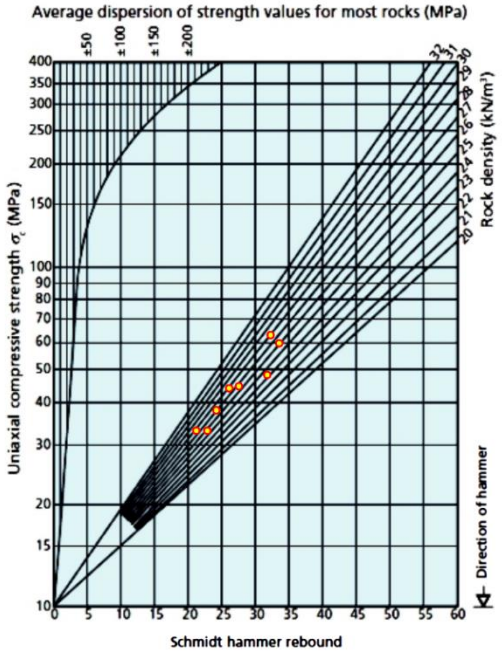

Fig. 5. Plotting of SRN and density of the studied samples on the Deere and Miller (1966) chart.

Table 3. The results of physical and geotechnical characterization of the studied samples.

Block ID	UPV (m/s)	Bulk density (g/cm³)	Solid density (g/cm³)	Total porosity (%)	Absorption (%)	SRN	UCS (MPa)
S1A	2804	2.84	3.77	24.18	6.51	32.33	62.11
S1B	3134	2.64	3.58	26.02	7.77	33.67	58.58
S2A	2248	2.69	3.75	29.07	9.89	27.67	43.87
S2B	2190	2.82	3.77	25.68	8.34	26.17	43.32
S3A	2750	2.60	3.78	34.44	9.39	22.92	32.60
S3B	2812	2.46	3.68	36.77	9.63	31.82	47.37
S4A	2532	2.73	3.79	24.00	7.32	24.30	37.31
S4B	2320	2.76	3.72	26.39	9.17	21.45	32.35
Min.	2190	2.46	3.58	24.00	6.51	21.45	32.35
Max.	3134	2.84	3.79	36.77	9.89	33.67	62.11
Aver.	2599	2.69	3.73	28.32	8.50	27.54	44.69

3.4 Slaking Durability Index

The slaking durability test revealed that the slaking durability index after the fourth cycle (I_{d4}) ranging between 88.99 and 94.98 %, while their average value is 92.52 % (Table 4). Obviously, S3A samples have the highest I_{d4}, while S2B samples have the lowest I_{d4}.

According to the durability classification proposed by Gamble (1971) and recommended by ISRM (Ulusay and Hudson, 2007), most of the studied samples are classified as medium high to high durable rocks (Table 4).

Table 4. The results of slaking durability test.

Sample	Slaking durability index (%) after				ISRM Durability classification
	First cycle (I_{d1})	Second cycle (I_{d2})	Third cycle (I_{d3})	Fourth cycle (I_{d4})	
S1A	98.02	96.04	94.86	93.60	High
S1B	98.05	96.11	94.87	93.33	High
S2A	97.48	94.96	93.40	91.77	Medium High
S2B	96.25	92.51	90.68	88.99	Medium High
S3A	98.22	96.45	95.46	94.21	High
S3B	98.37	96.74	95.99	94.98	High
S4A	97.25	94.50	93.44	92.18	Medium High
S4B	97.16	94.32	92.72	91.13	Medium High
Ave.	97. 60	95.20	93.92	92.52	Medium High

Examining the influence of slaking cycles on the slaking durability index (Fig. 6), it was revealed that as the number of cycles increased, the retained weight of the samples decreased in all cases. The rate at which the slaking-durability index decreased at the initial cycles (I_{d1}) was higher than the rate for the remaining cycles. After the first cycle, the slaking-durability index curves became almost linear until the fourth cycle, indicating that the slaking behavior was stable with respect to wetting and drying cycles for the samples tested.

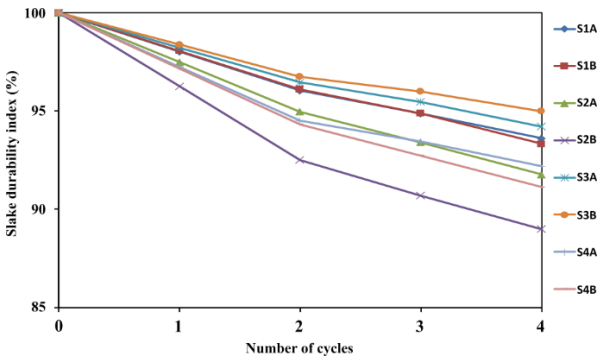

Fig. 6. The effect of the number of slaking cycles on the slaking durability index of the studied samples.

The appearance of fragments retained in the drum after completing the slaking durability test was photographed. These photographs were compared with the ASTM (1996) classification system to be categorized. Most of the studied samples were determined to be Type I and Type II material (Fig. 7).

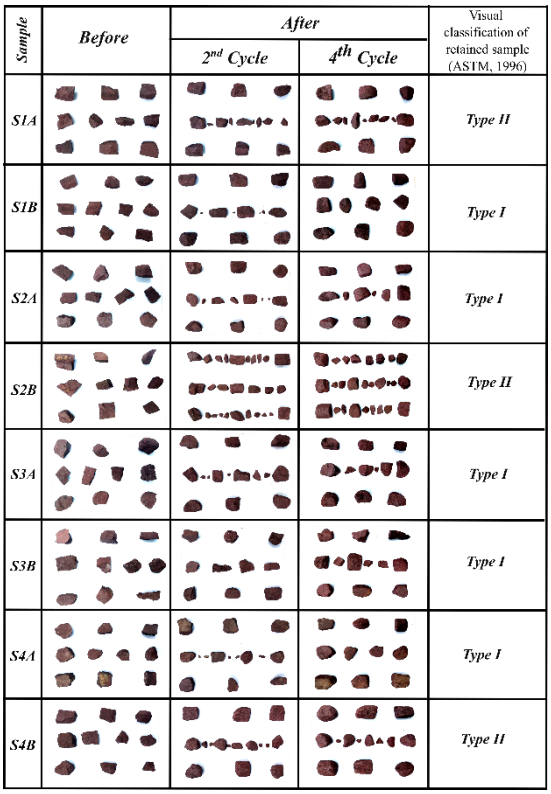

Fig. 7. Photographs of the studied samples and their retained fragments after the 2nd and 4th cycles of slaking durability tests and their visual classification according to ASTM, 1996.

Based on the slaking durability test results and the correlation of I_{d2} with the studied variables (Table 5), there are several factors that significantly influence the slaking durability of studied ooidal ironstone, these factors can be summarized as follows:

Geochemistry and mineralogy: The mineral and the chemical composition of ooidal ironstone play primary role. Clay minerals, particularly kaolinite, are susceptible to water absorption and water sensitive minerals, which cause the breakdown of certain samples, such as S1A. In contrast, apatite helps improve slaking durability, making some samples, such as S3B, more durable. The relative abundance of these minerals significantly influences overall stability, this is supported by the strong positive correlation of the I_{d_2} with P_2O_5 and CaO, while I_{d_2} shows a negative correlation with Fe_2O_3 and Al_2O_3.

Table 5. The correlation and determination coefficients of the I_{d2} with the other studied variables.

Variable	Correlations coefficient (r)	Determination coefficient (R^2)
Absorption	0.14	0.02
Bulk density	-0.65	0.43
Solid density	-0.31	0.10
Porosity	0.65	0.42
UPV	0.87	0.76
SRN	0.67	0.45
UCS	0.04	0.00
SiO_2	-0.11	0.01
Al_2O_3	-0.45	0.20
P_2O_5	0.87	0.76
Fe_2O_3	-0.52	0.27
CaO	0.82	0.67

Cementing material: The type and the amount of cementing material that binds grains together also influences slaking durability of the samples studied. Apatite cemented samples, such as S3B, are more durable than hematite or clay cemented samples, such as S1A.

Porosity: Surprisingly, higher porosity correlated with increased durability in the tested samples. This might be because highly porous rocks can hold more cementing agents, which fill in the pore spaces and enhance structural integrity. This finding is further supported by the wide variation in bulk density, porosity and UPV values.

Weathering: Pre-existing weathering can significantly reduce the slaking durability of rocks. Weathering processes can break down cementing materials, increase porosity, and introduce microfractures. These pre-existing weaknesses make the rock more vulnerable to further breakdown during wetting and drying cycles.

By considering these key factors, researchers and engineers can more accurately predict the behavior of ooidal ironstones under varying conditions. Notably, the strong correlation between UPV, SRN, and I_{d2}, suggests that these parameters providing a practical tool for field assessments of slaking durability.

5. Conclusions

In conclusion, Aswan's ooidal ironstones are primarily composed of hematite and quartz, with minor or trace amounts of kaolinite, fluorapatite, goethite, and rutile. These mineralogical characteristics, along with the observed high porosity and low bulk density, are consistent with characteristics of such rocks, ooidal texture, and their chemical composition.

The ultrasonic P-wave velocity (UPV) results, which ranged between 1911 and 3275 m/s, with an average of 2590 m/s. Most samples show medium to high slake durability (I_{d2}: 92.51–96.74%), indicating their potential suitability for construction and infrastructure applications.

A strong correlation was found between slake durability and several factors including mineral composition-particularly the presence of apatite-as well as physical properties such as porosity, bulk density, and water absorption. Furthermore, the durability of the studied ooidal ironstones was significantly influenced by geochemical components such as elevated P_2O_5 and CaO contents.

The study also highlighted that slake durability can be reliably estimated through UPV and SRN measurements, offering a practical tool for preliminary durability assessment.

From an application perspective, the results suggest that ooidal ironstones, particularly those rich in apatite, can be showed potential for specialized uses such as high-performance concrete in radiation shielding structures. Overall, this research contributes to a better

understanding of ooidal ironstone slaking behavior and supports its sustainable and effective use in construction, especially where long-term durability and resilience are critical.

Ethics approval and consent to participate: This article does not contain any studies with human participants or animals performed by any of the authors.

Consent for publication: All authors declare their consent for publication.

Conflicts of Interest: The author declares no conflict of interest.

Contribution of Authors: All authors shared in writing, editing and revising the MS and agree to its publication.

4. References

American Society of Testing and Materials (ASTM). (1996). Annual Book of ASTM Standards, Soil and Rock: Vol. 4.08, Section 4, ASTM, West Conshohocken, PA, 950 p.

Aydin, A. (2009). ISRM Suggested method for determination of the Schmidt hammer rebound hardness: Revised version. *International Journal of Rock Mechanics and Mining Sciences*, *46*(3), 627-634.

Aydin, A. (2014). Upgraded ISRM suggested method for determining sound velocity by ultrasonic pulse transmission technique. In *The ISRM Suggested Methods for Rock Characterization, Testing and Monitoring: 2007-2014* (pp. 95-99). Cham: Springer International Publishing.

Baioumy, H., Omran, M., & Fabritius, T. (2017). Mineralogy, geochemistry and the origin of high-phosphorus ooidal iron ores of Aswan, Egypt. *Ore Geology Reviews*, *80*, 185-199.

Balamadeswaran, P., & Mishra, A. K. (2020). Controlled blasting practices in quarries for sustainability: a case study. *Journal of Mines, Metals & Fuels*, *68*(8).

Bamber, A. S. (2008). *Integrated mining, pre-concentration and waste disposal systems for the increased sustainability of hard rock metal mining* (Doctoral dissertation, University of British Columbia).

Bhattacharyya, D. P. (1989). Concentrated and lean oolites: examples from the Nubia Formation at Aswan, Egypt, and significance of the oolite types in ironstone genesis. *Geological Society, London, Special Publications*, *46*(1), 93-103.

Brown, E. T. (1981). Rock characterization, testing & monitoring: ISRM suggested methods. *Pergamon Press, Oxford*, 81-89.

Daoud, A. M., Rashed, M. A., Elsharief, A. M., Sediek, K. N., & Elamein, A. M. (2020). The geotechnical properties of the oolitic ironstone formation, Wadi Halfa, North Sudan. *Journal of Geology and Mining Research*, *12*(1), 25-34.

Deere, D. U., & Miller, R. P. (1966). *Engineering classification and index properties for intact rock* (pp. 65-116). Springfield, VA, USA: National Technical Information Service.

El Aref, M. M., El Sharkawi, M. A., & Mesaed, A. A. (1996). Depositional and diagenetic microfabric evolution of the cretaceous ooidal ironstone of Aswan, Egypt. *Geological Society of Egypt*, 279-312.

Erguler, Z. A., & Ulusay, R. (2009). Assessment of physical disintegration characteristics of clay-bearing rocks: Disintegration index test and a new durability classification chart. *Engineering Geology*, *105*(1-2), 11-19.

Gamble, J. C. (1971). *Durability-Plasticity Classification of Shales and Other Argillaceous Rocks* (Doctoral dissertation, University of Illinois at Urbana-Champaign).

Gökceoğlu, C., Ulusay, R., & Sönmez, H. (2000). Factors affecting the durability of selected weak and clay-bearing rocks from Turkey, with particular emphasis on the influence of the number of drying and wetting cycles. *Engineering Geology*, *57*(3-4), 215-237.

Hanson C., Thomas D., & Gallagher B. (2005), The Value of Early Geotechnical Assessment in Mine Planning, in Naj Aziz and Bob Kininmonth (eds.), Proceedings of the 2005 Coal Operators' Conference, Mining Engineering, University of Wollongong, 18-20.

Horsfall, O. I., Omubo-Pepple, V. B., & Tamunobereton-ari, I. (2013). Correlation analysis between sonic and density logs for porosity determination in the south-eastern part of the Niger Delta Basin of Nigeria. *Asian Journal of Science and Technology*, *4*(1), 1-5.

Hu, L., Wu, H., Zhang, L., Zhang, P., & Wen, Q. (2017). Geotechnical properties of mine tailings. *Journal of Materials in Civil Engineering*, *29*(2), 04016220.

Hussein, A.A.A. Sharkawi M.A.E. Mineral deposits. R. Said (Ed.), The Geology of Egypt, 1, A.A. Balkema Publishers, Rotterdam, Netherlands (1990), pp. 511-566.

Klitzsch, E. (1986). Plate tectonics and cratonal geology in Northeast Africa (Egypt, Sudan). *Geologische Rundschau*, *75*, 755-768.

Klitzsch, E., List, F. K., and Pohlmann, G. (1987). ‘‘Geological Map of Egypt, Luxor and Gebel Hamata Sheets: Scale 1:500,000.’’ The Egyptian General Petroleum Corporation/Conoco, Cairo, Egypt.

Mekkawi, M. M., El Emam, A. E., Taha, A. I., Al Deep, M. A., Araffa, S. A. S., Massoud, U. S., & Abbas, A. M. (2021). Integrated geophysical approach in exploration of iron ore deposits in the North-eastern Aswan-Egypt: a case study. *Arabian Journal of Geosciences*, *14*(8), 721.

Mücke, A. (2000). Environmental conditions in the Late Cretaceous African Tethys: conclusions from a microscopic-microchemical study of ooidal ironstones from Egypt, Sudan and Nigeria. *Journal of African Earth Sciences*, *30*(1), 25-46.

Mücke, A., & Farshad, F. (2005). Whole-rock and mineralogical composition of Phanerozoic ooidal ironstones: Comparison and differentiation of types and subtypes. *Ore Geology Reviews*, *26*(3-4), 227-262.

Nwaiwu, C. M. O., Alkali, I. B. K., & Ahmed, U. A. (2006). Properties of ironstone lateritic gravels in relation to gravel road pavement construction. *Geotechnical & Geological Engineering*, *24*, 283-298.

Petránek, J., & Van Houten, F. B. (1997). *Phanerozoic Ooidal Ironstones: Contribution to the International Geological Correlation Programme: Project 277-Phanerozoic Ooidal Ironstones* (7). Czech geological survey.

Rahimi, B., Sharifzadeh, M., & Feng, X. T. (2021). A comprehensive underground excavation design (CUED) methodology for geotechnical engineering design of deep underground mining and tunneling. *International Journal of Rock Mechanics and Mining Sciences*, *143*, 104684.

Salama, W. (2014). Paleoenvironmental significance of aluminum phosphate-sulfate minerals in the upper Cretaceous ooidal ironstones, E-NE Aswan area, southern Egypt. *International Journal of Earth Sciences*, *103*, 1621-1639.

Selen, L., Panthi, K. K., & Vistnes, G. (2020). An analysis on the slaking and disintegration extent of weak rock mass of the water tunnels for hydropower project using modified slake durability test. *Bulletin of Engineering Geology and the Environment*, *79*, 1919-1937.

Singh, A., Singh, V., Patra, S., Dixit, P., & Mukherjee, A. K. (2024). Review on high phosphorous in iron ore: problem and way out. *Mining, Metallurgy & Exploration*, *41*(3), 1497-1507.

Young, T. P., Aggett, J. R., Howard, A. S., & Parsons, D. (1990). Field Guide No. 9. Jurassic and Ordovician Ooidal Ironstones. British Sedimentological Research Group. 13th International Sedimentological Congress, Nottingham U.K., pp. 32-50

Ulusay, R., & Hudson, J. A. (2007). International Society for Rock Mechanics (ISRM), the complete ISRM suggested methods for rock characterization, testing and monitoring, 1974–2006. Ankara.

Youssef MA (2018) Integrated geophysical prospecting of the iron ore deposits at east of Aswan, Upper Egypt. Ph. D. Thesis, Ain Shams University, 359 P.

Zorlu, K., & Yağız, S. (2018). Relationships between results of slake durability test and fractal dimension of aggregates. *Yerbilimleri/Earth Sciences*.

تقييم متانة الحجر الحديدي البطروخي في منطقة أسوان، مصر

هشام إسماعيل[١]، وكارم مبارك[١]، وكرم عبدالقادر[٢]، وعلى إسماعيل[١]

[١]قسم الجيولوجيا، كلية العلوم، جامعة جنوب الوادي، قنا، مصر

[٢] شركة جيوكويرى للتعدين، شارع التجارة، كورنيش النيل، أسوان، مصر

حجر الحديد البطروخي، وهو صخر رسوبي موجود في منطقة أسوان بمصر، تثير قابليته للتأثر بالتآكل والبري مخاوف بشأن أدائه طويل الأمد وملاءمته لتطبيقات البناء والبنية التحتية. تقيم هذه الدراسة متانة حجر الحديد البطروخي الموجودة في مكون التمساح من خلال اختبار المتانة القياسي. وقد تم إجراء تحليل مفصل أيضًا لخصائصه الفيزيائية والمعدنية والكيميائية لتحديد العوامل الرئيسية المؤثرة على المتانة. تُظهر النتائج أن أحجار الحديد البطروخي ذات مؤشرات متانة تتراوح بين متوسطة وعالية (I_{d2}: 92.51–96.74%). كما وُجد ارتباط قوي بين مؤشر المتانة وعدة عوامل، بما في ذلك التركيب المعدني – وخاصةً وجود الأباتيت والكاولين – بالإضافة إلى خصائص فيزيائية مثل المسامية والكثافة الظاهرية وامتصاص الماء. علاوة على ذلك، يؤثر التركيب الكيميائي مثل ارتفاع نسب كلا من P_2O_5 وCaO بشكل إيجابي على المتانة. أثبتت الدراسة ايضا أن طرق الاختبار غير المدمرة، وخاصة سرعة الموجات فوق الصوتية، يمكنها التنبؤ بشكل موثوق بمؤشرات المتانة ($R^2 > 0.76$) للحجر الحديدي البطروخي، مما يوفر أدوات عملية للتقييم الميداني.